# Temperature sensitivity of the cavity scale factor enhancement for a Gaussian absorption resonance

Krishna Myneni, David D. Smith, Hongrok Chang, and H. A. Luckay

Phys. Rev. A **92**, 053845 — Published 19 November 2015

DOI: 10.1103/PhysRevA.92.053845

# Temperature Sensitivity of the Cavity Scale Factor Enhancement for a Gaussian Absorption Resonance

Krishna Myneni*

*U.S. Army Aviation and Missile Research, Development, and Engineering Center, Redstone Arsenal, AL 35898*

David D. Smith

*NASA Marshall Spaceflight Center, ES34, Huntsville, AL 35812*

Hongrok Chang

*Miltec, 678 Discovery Dr., Huntsville, AL 35806*

H. A. Luckay

*Jacobs Technology, ESSSA Group, Huntsville, AL 35812*

## Abstract

We derive analytic expressions for the on-resonant cavity scale factor enhancement dependence on temperature, $S_0(T)$, for an intracavity medium with a Gaussian absorption resonance. Results are expressed as functions of the cavity parameters and the two resonance parameters: $\alpha_0(T)$, the peak absorption coefficient, and $\Gamma_\alpha^R(T)$, the resonance width. A semi-empirical model is developed for the temperature-dependent absorption coefficient, $\alpha_F(\Delta, T)$, in an alkali atom vapor cell, and is used to compare the predicted behavior of $\alpha_0(T)$ and $\Gamma_\alpha^R(T)$ with the measured values for the $D_2$ $F = 2 \rightarrow F'$ resonance in $^{87}$Rb, over the temperature range 298–325 K. Measurements of $S_0(T)$ in a low-finesse ring cavity, using the same vapor cell as the intracavity dispersive medium, were performed and found to be in agreement with the temperature-dependent behavior predicted by our theory, with quantitative agreement to 2 K for the critical temperature. The practical range of $S_0$ is found to be limited by the achievable temperature stability of the resonance parameters of the dispersive medium.

PACS numbers: 32.70.Jz, 42.50.Ct, 42.60.Da

* krishna.myneni.civ@mail.mil

## I. INTRODUCTION

The change in the optical mode frequency of a cavity due to a change in cavity length may be increased by a large factor through the anomalous dispersion associated with the absorption resonance of an intracavity medium. Enhancement of the scale factor relating the mode frequency of the optical cavity to its optical path length may be useful for a number of precision measurement applications, such as higher sensitivity passive and active ring resonator gyroscopes (see [1] and references, therein; [2–4]). The scale factor enhancement, $S$, depends on the absorption profile and is greatest when the cavity mode is resonant with the absorption medium. In an earlier paper [1] we demonstrated tuning the on-resonant scale factor enhancement, $S_0$, of an optical cavity by modifying the absorption coefficient of an intracavity atomic vapor cell through optical hyperfine pumping. It was shown that $S_0$ could be tuned across a wide range, from near unity to above the pole in $S_0$, with a rubidium vapor cell at room temperature. However, a large value of $S_0$ alone is not useful without simultaneously achieving high scale factor stability, if sensitivity is to be increased.

In this paper, we derive the general temperature dependence of $S_0$ for any intracavity medium with a Gaussian absorption resonance, in which the resonance parameters, $\alpha_0$ and $\Gamma_\alpha^R$, the peak absorption coefficient and the full width at half maximum (FWHM) of the absorption coefficient profile, vary with temperature. Knowledge of the temperature-dependence of $S_0$ is useful when temperature is used as the tuning parameter, and is critical for estimating the scale factor stability in a dispersion-enhanced optical cavity, e.g. in a dispersion-enhanced ring gyro, since the stability of $S_0$ will be limited by the achievable temperature stability of the intracavity dispersive medium. We demonstrate an accurate semi-empirical model for the temperature-dependence of the Gaussian resonance parameters, applicable to our medium of interest, an atomic vapor cell containing isotopically selected rubidium ($^{87}$Rb), derive the temperature dependence of the scale-factor enhancement, $S_0(T)$, examine its stability, $\delta S_0/S_0$, and the usable range of $S_0$ for the case of temperature tuning, with the cavity and atomic vapor cell used in our work. We show that the temperature sensitivity of our resonance parameters limit the scale factor stability to about one part per thousand at room temperature, for any value of $S_0$.

## II. SEMI-EMPIRICAL TEMPERATURE-DEPENDENT RESONANCE PARAMETERS

In this section, we derive the semi-empirical temperature-dependence of the absorption resonance for the atomic medium used in our previous work, a low density thermal atomic vapor of alkali atoms confined to a glass vapor cell with a limited supply of atoms. The expressions will be useful for vapor cells of other species of atoms as well. First, we begin with a treatment of the absorption coefficient by a vapor of non-interacting two-level atoms. Then, the results are combined with an empirical model of the equilibrium density versus temperature for a metallic vapor to describe the temperature-dependent absorption coefficient profile of the optical resonances of alkali atoms, each consisting of multiple hyperfine transitions. The hyperfine splitting of the upper levels leads to resonances which are approximately Gaussian at our temperatures of interest, and may be characterized by Gaussian parameters, $\alpha_0(T)$ and $\Gamma_\alpha^R(T)$, in order to provide useful estimates of $S_0(T)$.

### A. Two-Level Atomic Vapor

For an ideal two-level atomic system at a density low enough where collisions may be ignored, the absorption resonance shape, $\alpha(\omega - \omega_0, T)$, is a Voigt function. Near room temperature, however, the inhomogeneous width is typically orders of magnitude larger than the homogeneous width for an optical resonance, and the resonance shape may be approximated as a Gaussian, given by,

$$\alpha(\Delta, T) \;=\; \alpha_0(T) \exp\left(-4 \ln 2 \frac{\Delta^2}{\Gamma_\alpha^2(T)}\right), \tag{1}$$

where $\Delta \equiv \omega - \omega_0$ is the optical frequency detuning from the resonance frequency, $\omega_0$, and $\alpha_0$ is the on-resonance absorption coefficient, $\Gamma_\alpha$ is the FWHM of the absorption coefficient profile, and $T$ is the temperature.

The functional dependence of $\Gamma_\alpha$ on temperature is given by the Doppler width formula,

$$\Gamma_\alpha(T) \;=\; \left(\frac{\omega_0}{c}\right)\left(\frac{8 k_B T \ln(2)}{m}\right)^{1/2}, \tag{2}$$

where $c$ is the speed of light, and $m$ is the mass of the atom. In the *low optical intensity limit*, the on-resonance absorption coefficient has a temperature dependence given by,

$$\alpha_0(T) \;=\; \mathbb{N}_\ell(T) \mathcal{F}_\ell(T) \sigma_0, \tag{3}$$

where $\sigma_0$ is the resonant absorption cross-section, $\mathbb{N}_\ell(T)$ is the number density of atoms in the vapor occupying the lower-level of the two-level atomic resonance, and $\mathcal{F}_\ell(T)$ is the fraction of lower-level atoms in the vapor which can absorb the beam on resonance, given by

$$\mathcal{F}_\ell(T) \;=\; \int_{-\infty}^{+\infty} L(\upsilon_z) P(\upsilon_z; T)\, d\upsilon_z. \tag{4}$$

where $L(\upsilon_z)$ is a velocity-dependent line-shape function, which, at low-intensity, is given by,

$$L(\upsilon_z) \;=\; \frac{(\gamma/2)^2}{(k\upsilon_z)^2 + (\gamma/2)^2} \tag{5}$$

and $P(\upsilon_z; T)$ is the probability density of an atom having velocity $\upsilon_z$ at temperature $T$,

$$P(\upsilon_z; T) \;=\; \frac{1}{\sqrt{\pi}\upsilon_p(T)} \exp\left(-\upsilon_z^2/\upsilon_p^2(T)\right) \tag{6}$$

with $\upsilon_p(T) \;=\; \sqrt{2k_B T/m}$. In eq. 5, $\gamma$ is the natural linewidth of the resonance, assuming conditions of negligible broadening by collisions and external fields, and $k$ is the wavenumber of the optical field. Defining $x(T) \;=\; \upsilon_\gamma/\upsilon_p(T)$, with $\upsilon_\gamma \;=\; \gamma/2k$, and carrying out the integration in eq. 4, the fraction of absorbing atoms with an on-resonant beam is given by,

$$\mathcal{F}_\ell(T) \;=\; \sqrt{\pi}\,\mathrm{erfc}\,(x)\, x \exp\left(x^2\right). \tag{7}$$

Note that in the limit $T \to 0$, $\mathcal{F}_\ell \to 1$, as expected.

### B. Alkali Atom Vapor Cell

For atoms completely in the vapor phase within a closed cell, $\mathbb{N}_\ell$ is constant with temperature; however, $\mathcal{F}_\ell(T)$ will decrease with increasing temperature, since a smaller fraction of the atoms in vapor will have near-zero velocity. As a result, $\alpha_0$ will correspondingly decrease with temperature. However, if the atomic system is partially in vapor phase and partially in liquid phase, at the high vacuum of typical vapor cells, $\mathbb{N}_\ell(T)$ increases with temperature as more atoms are added to the vapor. Henceforth, we restrict our discussion to the latter case of a very low pressure vapor of atoms in a cell containing a liquid phase reservoir at ambient temperature. This case corresponds approximately to commercially available vapor cells of several alkali atoms, including rubidium (Rb) cells containing no buffer gases. For

metallic elements the vapor pressure versus temperature may be represented by a two-term equation given in [5],

$$\log(p) \approx A + BT^{-1}, \tag{8}$$

where $p$ is in units of atm, and $T$ is in Kelvin. For rubidium in liquid phase, vapor pressure measurements give the constants $A$ =4.312, and $B$ =-4040 [5]. This form has an accuracy of 5% over the range 298–550K. In S.I. units, the atom density is given by[6],

$$\mathbb{N}(T) = \frac{133.3}{k_B T} \times 10^{\{2.881 + A + B/T\}}, \tag{9}$$

where $T$ is specified in Kelvin. The vapor pressure parameters $A$ and $B$ are obtained by measurement under conditions which often do not closely correspond with vapor pressures in commercial atomic vapor cells, due to wall effects [7]. Typical alkali vapor cells also contain a very limited amount of the condensed phase element, and, for temperatures well above room temperature, the vapor pressure may be limited by the available quantity of the element. For example, in some commercial rubidium vapor cells, liquid phase rubidium is not even visible on the cell wall at room temperature. For an overfilled cell at room temperature, i.e. one in which the liquid is visibly condensed on the wall of the cell, we model the vapor pressure (atom density) in the cell by determining the parameters $A$ and $B$ by optical measurements of the absorption coefficient for atomic transitions with known absorption cross sections.

Alkali atoms exhibit a splitting of the ground state into two hyperfine levels, separated by more than $k_B T$ at room temperature, but not so great that the Boltzmann factor is significantly different between the two levels. The number density of atoms in thermal equilibrium, in the lower level, is given by,

$$\mathbb{N}_\ell(T) = \left( \frac{2F+1}{\sum_{F_g} 2F_g + 1} \right) \mathbb{N}(T), \tag{10}$$

where $F$ is the total angular momentum quantum number of the lower level, and the summation extends over the two hyperfine levels of the ground state. It is also noted that $\sigma_0$, the resonant absorption cross section, in a real atom depends on the polarization of the incident beam, and on the distribution of the lower level atoms within their degenerate magnetic sublevels. Also, optical pumping effects within the lower sublevels, even at low incident intensities, may significantly alter the sublevel populations for sufficient atom-beam

interaction time[8], and thereby modify $\sigma_0$. For a specific hyperfine transition, $F \rightarrow F'$,

$$\sigma_0(F, F') \;=\; \frac{2\omega \left|\mu_{FF',e}\right|^2}{c\epsilon_0 \hbar \gamma}, \tag{11}$$

where $\mu_{FF',e}$ is the effective dipole moment for the transition between the two hyperfine levels. For linear polarization, $\mu_{FF',e}$ is given by,

$$\left|\mu_{FF',e}\right|^2 \;=\; \sum_{m=-F}^{+F} w_m \left|\langle F, m \left| er_{q=0} \right| F', m\rangle\right|^2 \tag{12}$$

and $w_m$ specifies the weights for the distribution of atoms within the lower magnetic sublevels. Assuming the incident beam intensity and interaction time are sufficiently low such that the ground state atom does not depart significantly from thermal equilibrium, we may take $w_m = 1/(2F+1)$ and calculate the effective resonant linear polarization absorption cross sections through application of the Wigner-Eckart theorem[6], to give

$$\sigma_0^{\pi}(F, F') \;=\; s(F, F')\sigma_0^{\pi}(F), \tag{13}$$

where $s(F, F')$ are the relative strengths for the individual $F \rightarrow F'$ hyperfine transitions, and $\sigma_0^{\pi}(F)$ is given by,

$$\sigma_0^{\pi}(F) \;=\; \frac{2}{3}\frac{\omega_F}{c\epsilon_0 \hbar \gamma} \left|\langle J \parallel er \parallel J'\rangle\right|^2 \tag{14}$$

and $\omega_F$ is the center frequency of all transitions from the lower common level $F$ to the multiple upper levels, $F'$, of the excited state. For the $F = 2 \rightarrow F'$ $D_2$ resonance of $^{87}$Rb, considered in this work, $\sigma_0^{\pi}(2) \;=\; 19.378 \times 10^{-14}\mathrm{m}^2$, and $s(2,1) = 0.05$, $s(2,2) = 0.25$, and $s(2,3) = 0.70$[6]. Combining equations 1, 3, and 14, and summing over all of the excited state hyperfine levels $F'$, we obtain the temperature and frequency detuning dependent absorption coefficient profile for the composite resonance, $F \rightarrow F'$, with common lower level $F$,

$$\alpha_F(\Delta, T) \;=\; \alpha_D(T) \sum_{F'} s(F, F') \exp\left(-4\ln 2 \left(\frac{\Delta + \delta_{F,F'}}{\Gamma_\alpha(T)}\right)^2\right), \tag{15}$$

where the detuning, $\Delta = \omega - \omega_{F,F_r'}$, is with respect to the $F \rightarrow F_r'$ transition, $F_r'$ is the reference hyperfine level in the excited state, $\delta_{F,F'} = \omega_{F,F_r'} - \omega_{F,F'}$, $\Gamma_\alpha(T)$ is given by eq. 2, and $\alpha_D(T)$ is given by,

$$\alpha_D(T) \;=\; N_\ell(T)\mathcal{F}_\ell(T)\sigma_0^{\pi}(F). \tag{16}$$

It is worthwhile to review all of the assumptions used to obtain equation 15: 1) the natural linewidth is assumed to be much smaller than the Doppler width, $\gamma \ll \Gamma_\alpha(T)$, 2)

there are no other significant line broadening mechanisms, 3) linear optical polarization is used, 4) the intensity is low enough that all levels and sublevel populations are always near thermal equilibrium, i.e. saturation and pumping effects are negligible, 5) external magnetic fields are negligible, i.e. Zeeman sublevel splitting is much less than the natural linewidth, and 6) the variation in $\omega_{F,F'}$ is negligible over the range of the upper levels, $F'$, so that $\omega_{F,F'}$ may be replaced simply by $\omega_F$(see eq. 14). For the rubidium vapor cell, near or above room temperature, and for the transitions, laser intensity, beam diameter, and polarization used in our experiments, these assumptions are well justified. However, in comparing our measurement results with theory, we will also include the contribution of the natural linewidth in an empirical way, since it is an inseparable contribution to the data, at the level of 0.5% in the resonance FWHM.

We have obtained a semi-empirical model of the absorption coefficient profile, eq. 15, for a composite resonance in a low-density alkali vapor cell near room temperature, and at very low incident intensity. Although the resonance is an unresolved blend of multiple displaced hyperfine components at room temperature, for the $5P_{3/2}$ excited state of $^{87}$Rb the close spacing of the upper $F'$ levels results in a nearly Gaussian absorption profile, with an asymmetry. To a reasonable approximation, we may treat the single $F \rightarrow$ multiple $F'$ composite resonance as an ideal Gaussian resonance and characterize $\alpha_F(\Delta, T)$ using just two parameters, $\alpha_0(T)$ and $\Gamma_\alpha^R(T)$. Although it is not possible to obtain simple analytic expressions for $\alpha_0(T)$ and $\Gamma_\alpha^R(T)$ for the composite resonance, we may obtain these two characteristic parameters by numerically computing the absorption cross section profile from our semi-empirical model (eq. 15) and finding its peak value and FWHM. We now proceed to determine the theoretical temperature dependence of the on-resonance cavity scale factor enhancement, $S_0(T)$, as a function of Gaussian resonance parameters, $\alpha_0(T)$ and $\Gamma_\alpha^R(T)$.

## III. TEMPERATURE DEPENDENCE OF SCALE FACTOR ENHANCEMENT

For an optical cavity, either in the linear configuration or a ring configuration, the Gaussian resonant medium may not fill the entire physical path-length through the cavity. In this case, we use an *effective absorption coefficient*,

$$\hat{\alpha}(\Delta, T) \;=\; \alpha(\Delta, T)\ell/L. \tag{17}$$

The parameters $\ell$ and $L$ are the length of the medium and length of the empty cavity, respectively, defined for one round-trip traversal of the cavity by the optical beam[9]. Thus, if $\ell_m$ is defined to be the physical length of the dispersive medium, $\ell = 2\ell_m$ for the Fabry-Perót cavity, and $\ell = \ell_m$ for a ring cavity, since the dispersive medium is traversed twice in one round-trip through the Fabry-Perót cavity, while it is traversed only once in a round-trip of the ring cavity. Similarly, $L$ is twice the mirror separation for a Fabry-Perót cavity, while, for a ring cavity, $L$ is its perimeter. This convention for $\ell$ and $L$ allows us to write expressions for $S$ which are valid for both cavity cases.

We generalize our earlier expression for the scale factor enhancement of an optical cavity with an intracavity absorber[1] to describe its temperature dependence,

$$S(\delta_p, T) \;=\; \left(\hat{n}_g(\Delta_p, T) + (1/t_c)\left(dF(\Delta_p, T)/d\Delta_p\right)\right)^{-1}, \tag{18}$$

where $\delta_p \equiv \omega_{p,ec} - \omega_o$ is the empty cavity mode detuning for mode $p$, $\Delta_p \equiv \omega_p - \omega_0$ is the corresponding dispersive cavity mode tuning, $\hat{n}_g(\Delta_p, T)$ is the *effective group index* at a detuning of $\Delta_p$, $t_c$ is the empty cavity round-trip time $(L/c)$, and $F(\Delta_p, T)$ is a function which depends on the temperature-dependent absorption resonance shape *and* on the cavity mode profile[1].

First, we obtain an approximate expression for $S_0(T)$, valid in the limit of narrow cavity mode-width. The simple expression obtained for this case is useful for obtaining insight into the behavior of $S_0(T)$ and for its rate of change with temperature, $dS_0/dT$. We also present the general expression for $S_0(T)$, valid when the cavity mode width is not small compared to the absorption resonance width. The latter is needed for a quantitative comparison of the theory with our present experiment.

### A. High-Finesse Approximation

In the limit that the cavity mode width is much narrower than the absorption resonance width, we may ignore the group velocity dispersion arising from $F(\Delta_p, g)$[1] to obtain the *high-finesse approximation*,

$$S(\delta_p, T) \;\approx\; \frac{1}{\hat{n}_g(\Delta_p, T)}, \tag{19}$$

where

$$\hat{n}_g(\Delta_p, T) \;=\; \hat{n}(\Delta_p, T) + \omega_p \left(\frac{\partial \hat{n}(\Delta, T)}{\partial \Delta}\right)\Bigg|_{\Delta=\Delta_p}. \tag{20}$$

Through the Kramers-Krönig relations, the effective medium index of refraction, $\hat{n}(\Delta, T)$, is related to the effective absorption coefficient, $\hat{\alpha}(\Delta, T)$, and resonance width, $\mathit{\Gamma}_{\alpha}^{R}(T)$, via,

$$\hat{n}(\Delta, T) = 1 + Re\left\{\frac{ic}{2}\frac{\hat{\alpha}(\Delta, T)}{(\Delta + \omega_0)}\mathrm{erf}\left(i2\ln 2\frac{\Delta}{\Gamma_{\alpha}^{R}(T)}\right)\right\}. \tag{21}$$

Below, we derive the on-resonance ($\Delta = 0$) scale factor enhancement temperature dependence, $S_0(T)$.

The temperature-dependence of the on-resonant group index, $\hat{n}_g$(0,T), is expressed only in terms of the two Gaussian absorption resonance parameters, $\hat{\alpha}_0(T)$ and $\Gamma_{\alpha}^{R}(T)$. From eq. 20,

$$\hat{n}_g(0, T) = \hat{n}(0, T) + \omega_0 \left.\frac{\partial \hat{n}(\Delta, T)}{\partial \Delta}\right|_{\Delta=0}. \tag{22}$$

From equation 21,

$$\left.\frac{\partial \hat{n}(\Delta, T)}{\partial \Delta}\right|_{\Delta=0} = -\frac{2c}{\omega_0}\sqrt{\frac{\ln 2}{\pi}}\frac{\hat{\alpha}_0(T)}{\Gamma_{\alpha}^{R}(T)}. \tag{23}$$

Finally, noting $\hat{n}(0, T) = 1$ for all temperatures, we obtain for $\hat{n}_g(0, T)$,

$$\hat{n}_g(0, T) \;=\; 1 - f\frac{\hat{\alpha}_0(T)}{\Gamma_{\alpha}^{R}(T)}, \tag{24}$$

where $f \;=\; 2c\sqrt{\ln(2)/\pi}$, and $c$ is the speed of light in vacuum. Substituting eq. 24 into eq. 19, the on-resonant scale factor enhancement, $S(\delta_p = 0, T)$, is

$$S_0(T) \;=\; \frac{1}{1 - f\frac{\hat{\alpha}_0(T)}{\Gamma_{\alpha}^{R}(T)}}. \tag{25}$$

The critical temperature, $T_c$, at which the pole in $S_0(T)$ occurs is given by the condition, $\Gamma_{\alpha}^{R}(T_c) = f\hat{\alpha}_0(T_c)$, which can be solved numerically, using equations 2, and 3.

From eq. 19, the rate of change of $S_0(T)$ with temperature is given by,

$$\frac{dS_0(T)}{dT} \;=\; -S_0^2(T)\frac{d\hat{n}_g(0, T)}{dT} \tag{26}$$

and, assuming no variation in the length ratio $\ell/L$ with temperature, we arrive at

$$\frac{dS_0(T)}{dT} \;=\; S_0^2(T)\cdot f\frac{\hat{\alpha}_0(T)}{\Gamma_{\alpha}^{R}(T)}\left[\frac{1}{\alpha_0(T)}\frac{d\alpha_0(T)}{dT} \;-\; \frac{1}{\Gamma_{\alpha}^{R}(T)}\frac{d\Gamma_{\alpha}^{R}(T)}{dT}\right]. \tag{27}$$

In the above expression, the only parameters are the two parameters characterizing the Gaussian absorption resonance, $\hat{\alpha}_0(T)$ and $\Gamma_{\alpha}^{R}(T)$. This is not surprising because the effective group index, $\hat{n}_g(0, T)$, is completely determined by these two parameters, for the Gaussian absorption resonance. From equation 27, we see that in order for $S_0$ to increase

with temperature, the fractional change in the on-resonance absorption coefficient, $\alpha_0$, must be greater than the fractional change in the width of the resonance, $\Gamma_\alpha^R$, for a small change in temperature. It is also possible, in principle, for $S_0$ to be independent of temperature if the term in brackets in eq. 27 becomes zero, i.e. when the fractional change in $\alpha_0$ is exactly the same as the fractional change in $\Gamma_\alpha^R$; however, for our atomic vapor cell, the fractional change in $\alpha_0$ is considerably greater than that of $\Gamma_\alpha^R$ over the temperature range of our measurements.

### B. General Expression

When the cavity mode width is not small compared to the absorption resonance width, higher-order dispersion across the cavity mode may significantly increase the value of $S_0$[1, 9]. Thus, in the general case, we cannot ignore the contribution from the term, $dF(\Delta_p, g)/d\Delta_p$, in eq. 18. Although the expression for $F(\Delta_p, g)$ is complicated, it is straightforward to evaluate $dF(\Delta_p, g)/d\Delta_p$ on resonance, i.e. for $\Delta_p = 0$, and therefore to find the contribution to $S_0$ from this term. The expression for $F(\Delta_p, g)$ given in [1] is valid only for transmittance of the optical field incident on the cavity. However, the cavity modes may also be observed in reflectance, and, for an empty cavity, the mode pattern will simply be inverted, with the transmittance maxima coinciding exactly in frequency with the minima in reflectance. This is also true in the high finesse approximation. However, with a resonant intracavity medium and a cavity with arbitrary finesse, the minimum of a reflectance mode may no longer coincide, in general, with the maximum of the corresponding transmittance mode.

The expressions for $F(\Delta_p, g)$ for both transmittance and reflectance are given in [10]. We denote the on-resonant scale factor enhancements, determined from the mode behavior observed in transmittance and in reflectance by $S_0^{\Im}$ and $S_0^{\Re}$, respectively. Consider a four mirror ring cavity, as shown in figure 1. The input coupler has a reflection coefficient $r_1$ and the output coupler a reflection coefficient of $r_2$. For modes observed in transmittance,

$$S_0^{\Im}(T) = \left( \hat{n}_g(0,T) - \frac{1}{t_c^2} \frac{4L \ln 2}{\hat{n}_g(0,T)} \frac{\hat{\alpha}_0(T)}{\left(\Gamma_\alpha^R(T)\right)^2} \left( \frac{1 - g_0^2(T)}{2 g_0(T)} \right) \right)^{-1}, \tag{28}$$

where $g_0(T) = r_1 r_2 a \tau_0(T)$, and $\tau_0(T) = \exp\left(-\hat{\alpha}_0(T) L/2\right)$. The cavity parameter, $a$, is the frequency-independent round-trip field attenuation in the cavity, which can include transmission losses from the cavity mirrors not designated as the input/output couplers. Note

that the second term on the right hand side of eq. 28 always lowers the value of $\hat{n}_g(0,T)$, for $0 \leqslant \hat{n}_g(0,T) \leqslant 1$, and therefore increases the value of $S_0^{\Im}$ at a given temperature. The connection between the general expression, eq. 28, and the high-finesse result, eq. 25, is seen by taking the limit $g_0 \to 1$.

The scale factor enhancement of the cavity observed in reflectance, $S_0^{\Re}$, is given by

$$S_0^{\Re}(T) = \left( \hat{n}_g(0,T) - \frac{1}{t_c^2} \frac{4L \ln 2}{\hat{n}_g(0,T)} \frac{\hat{\alpha}_0(T)}{\left(\Gamma_\alpha^R(T)\right)^2} \left( \frac{r_1^2 - g_0(T)}{r_1^2 - g_0^2(T)} \right) \frac{2g_0(T)}{1 + g_0(T)} \right)^{-1}. \qquad (29)$$

When $g_0(T) < r_1^2$, the effect of $dF(\Delta_p, g)/d\Delta_p$ on $S_0^{\Re}$ is to lower the value of $\hat{n}_g(0,T)$, as in eq. 28. However, the scale factor pole will occur at different temperatures for modes observed in reflectance rather than in transmittance. For ring cavity experiments, it may be more convenient to observe the cavity modes in reflectance than in transmittance, since $r_2$ can be set to near unity. In our experiments, described below, we measure $S_0^{\Re}(T)$ from a low-finesse ring cavity. We will use eq. 29 to evaluate the theoretical critical temperature, $T_c$, for comparison with our experiment. We will continue to use the notation $S_0$ for the cavity scale factor enhancement when the measurement type, transmittance or reflectance, is not germane to the discussion.

## IV. TEMPERATURE-DEPENDENT MEASUREMENTS

A low pressure vapor cell of $^{87}$Rb, of physical length, $\ell_m = 2.50 \pm 0.05$ cm, and having non-angled anti-reflection coated windows, was enclosed in a compact, temperature-stabilized aluminum oven, with a temperature tunable from room temperature, 298 K, to over 325 K. The atomic vapor cell is overfilled, so that condensed liquid rubidium droplets are visible on the cell wall at room temperature. The oven design was based on one previously published [11], and is heated by four cartridge heaters. A resistance temperature detector (RTD) sensor mounted on the outer surface of the oven provided an indirect measure of the vapor temperature, which is used by a temperature controller (Omega CN743) to stabilize the oven temperature to within 0.15 K. The systematic error between the average temperature of the atomic vapor and the measured oven temperature is not known precisely, but separate measurements of the temperature at various points inside the cell holder area of the oven indicate that the cell wall temperature was within 2 K of the oven measurement.

Measurements of both the temperature-dependent low-intensity absorption resonance

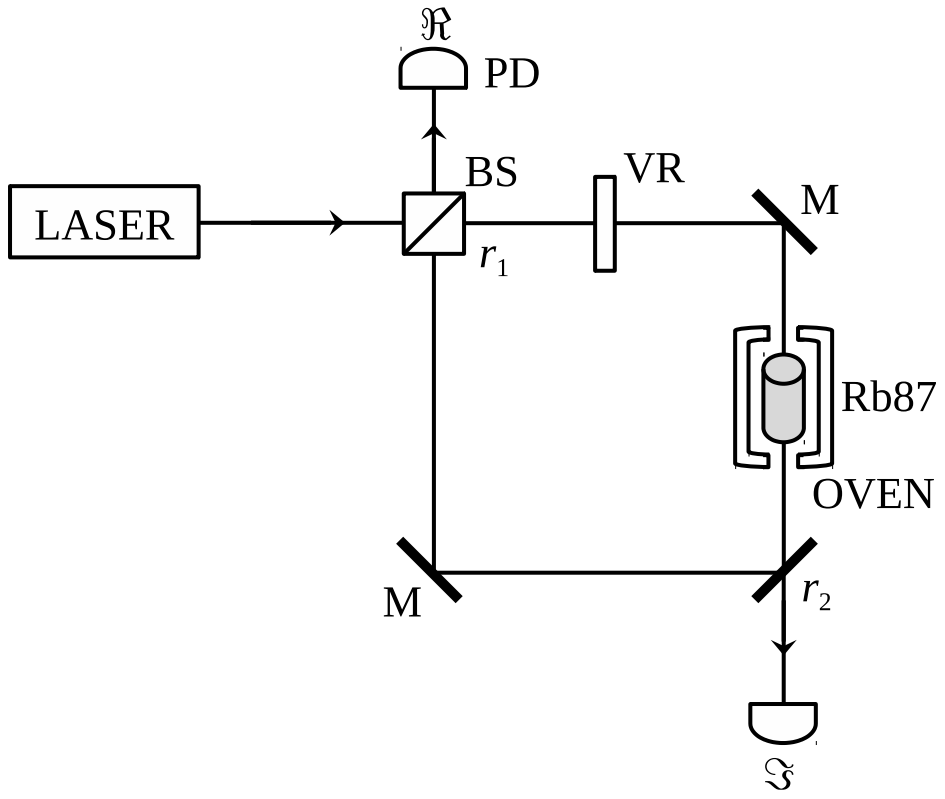


Figure 1. Ring cavity geometry for the general treatment of $S_0^{\Im}(T)$ and $S_0^{\Re}(T)$. In the layout, the laser enters the input coupler (BS) from only one direction, restricting the ring cavity to unidirectional operation. The intracavity, temperature-stabilized rubidium vapor cell provides anomalous dispersion at its $D$-line resonances. The liquid crystal variable retarder (VR) permits tuning the cavity mode across the atomic resonance, by changing the optical path length in the cavity. We measure for each temperature the $\Delta_p$ versus $\delta_p$ curve for the cavity mode $p$ closest to the atomic resonance frequency. In our experiment, the output coupler for the cavity is a high-reflectance mirror, $r_2 = 1$. Therefore, the input coupler also serves as an output coupler and allows only the cavity reflectance ($\Re$) modes to be observed by the photodetector (PD). The remaining two mirrors (M) of the ring cavity are high-reflectance mirrors.

parameters, $\alpha_0(T)$ and $\Gamma_\alpha^R(T)$, from the $D_2$ line and the on-resonance cavity scale factor enhancement, $S_0^{\Re}(T)$, were made using different optical configurations, as described below. Both sets of measurements used a tunable external-cavity diode laser operating near 780.2 nm. Absolute frequency scale calibration of spectra was provided by a Michelson interferometer and a saturated absorption (SA) spectrometer[1]. The frequency scale accu-

racy for the spectra in both sets of measurements was better than 0.4% across the entire resonance profile, as determined by the measured intervals between saturated-absorption resonances from the SA spectrometer.

### A. Absorption Resonance Parameters

For a low pressure vapor cell of $^{87}$Rb, measurements of the absorption resonance parameter, $\alpha_0$, at low intensity and near room temperature are given in [1]. In the present work, the dependence of $\alpha_0$ and $\Gamma_\alpha$ on temperature was measured over a wide temperature range. Single-pass transmittance spectra through the vapor cell were taken across the absorption profile of the $D_2$ $F = 2 \rightarrow F'$ resonance over a tuning range of $\pm 2.7$ GHz, and for temperatures ranging from 300–323 K. The input laser had a beam power of 44 nW and a $1/e$ beam radius of 310 $\mu$m, giving an average beam intensity of 15 $\mu$W/cm$^2$ incident on the vapor cell. A photomultiplier (ThorLabs PMM02-1) was used to detect the weak transmitted light. For the intensity and beam diameter used, both saturation and pumping effects are negligible ($\Omega/\gamma \approx 0.05$, and $\pi/\Omega \approx 2\mu$s, where $\Omega$ is the effective Rabi rate of the $2 \rightarrow 3$ transition, and $\gamma$ is the spontaneous emission decay rate).

For each temperature, the parameters $\alpha_D(T)$ and $\Gamma_\alpha(T)$ were obtained by a least-squares fit to the measured transmittance spectrum. The fitting function is obtained by substituting eq. 15 into the expression, $\mathcal{T}(\Delta, T) = \exp\left(-\alpha_F(\Delta, T)\ell_m\right)$. We emphasize that the least-squares fit should be performed to the measured transmittance spectra, $\mathcal{T}(\Delta, T)$, instead of computing $\alpha_F(\Delta, T)$ from the transmittance data and then performing a least-squares fit to $\alpha_F(\Delta, T)$. In the latter case, the measurements will be weighted incorrectly and give poor results for $\alpha_D(T)$ and $\Gamma_\alpha(T)$, particularly at higher temperatures. The parameter values, $\alpha_D(T)$, obtained from the transmittance measurements, were then fitted to the theoretical model, eq. 16 to obtain the density model parameters, $A$ and $B$. For our atomic vapor cell, we obtained $A = 3.485 \pm 0.133$ and $B = -3805 \pm 42$. Figure 2 shows transmittance spectra for three different vapor cell temperatures, fits to these curves, and the corresponding absorption coefficient curves.

As noted previously, $\alpha_D(T)$ and $\Gamma_\alpha(T)$ are not the direct parameters of interest for use with our model of $S_0(T)$ for a Gaussian resonance. The desired Gaussian parameters, $\alpha_0(T)$ and $\Gamma_\alpha^R(T)$, are obtained by finding the peak and FWHM of the composite resonance,

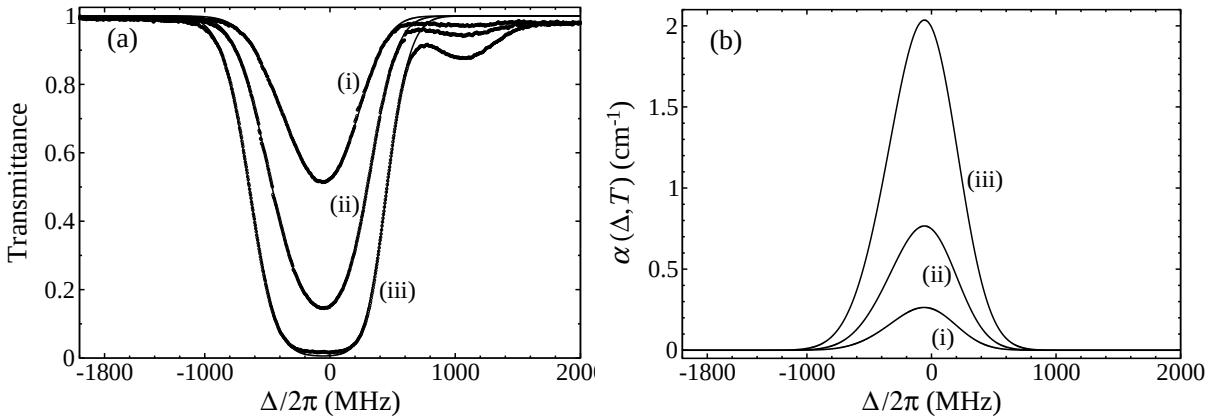


Figure 2. (a) Single-pass transmittance spectra, $\mathcal{T}(\Delta, T)$, through the rubidium vapor cell for three different temperatures: (i) 300 K, (ii) 311 K, and (iii) 323 K. The corresponding fits to $\exp(-\alpha_{F=2}(\Delta, T)\ell_m)$ are superimposed. The dip in transmittance at a detuning of +1100 MHz is due to absorption from $^{85}$Rb, and this region has been excluded from the fit. (b) Absorption coefficient spectra, $\alpha_{F=2}(\Delta, T)$, corresponding to the fitted curves in (a). Note the asymmetry in the absorption curves, arising from the multiple hyperfine transitions contributing to the resonance.

$\alpha_F(\Delta, T)$, computed with the fitted parameters, $\{\alpha_D(T),\, \Gamma_\alpha(T),\, A,\, B\}$, from our transmittance measurements. Figure 3 plots the measured and predicted $\alpha_0(T)$ and $\Gamma_\alpha^R(T)$ over the temperature range of the measurements. For this range, we find the following convenient empirical relation between $\alpha_D(T)$ and the peak absorption coefficient,

$$\alpha_0(T) \;=\; 0.8656 \times \alpha_D(T) \;-\; 0.763\,\mathrm{m}^{-1}. \tag{30}$$

We also find that within a limited temperature regime, 300–325 K, $\Gamma_\alpha^R(T)$, is well-described by a linear relation to the fitted two-level Doppler width, $\Gamma_\alpha(T)$,

$$\Gamma_\alpha^R(T) \;=\; 0.8705 \times \Gamma_\alpha(T) \;+\; 2\pi \times 161.1 \times 10^6\,\mathrm{s}^{-1}. \tag{31}$$

It should be noted that the two relations above do not connect experimental values to theoretical values, but provide simple means of calculating the experimental composite resonance parameters from the two fitted parameters to the experimental spectra. Comparison of the experimental $\alpha_0(T)$ and $\Gamma_\alpha^R(T)$ to the theory is shown in fig. 3, and discussed in section V.

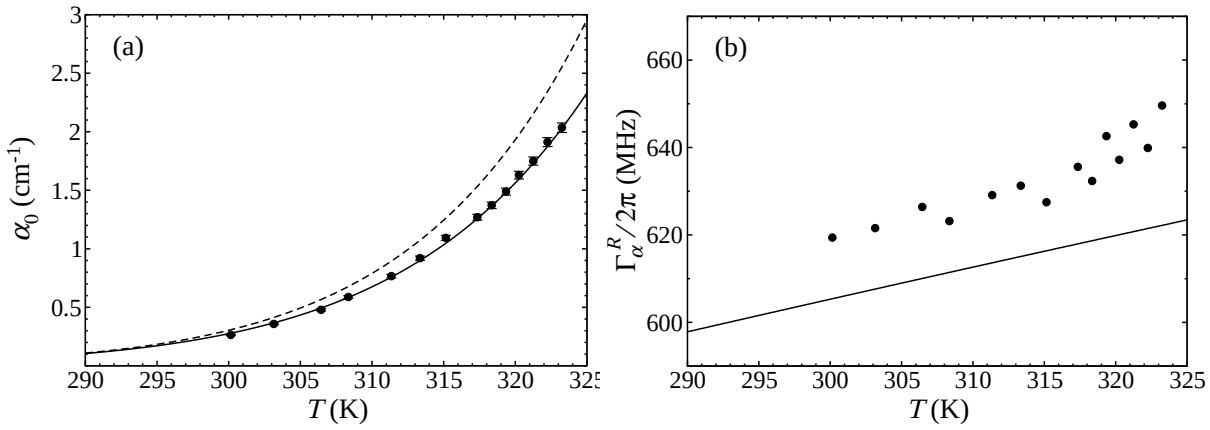


Figure 3. (a) Peak absorption coefficient, $\alpha_0(T)$, and (b) resonance FWHM, $\Gamma_\alpha^R(T)$, for the $D_2$ $F = 2 \rightarrow F'$ resonance. Points are experimental values while the lines are computed from the semi-empirical model (eq. 15). In (a), the solid line uses the vapor pressure parameters, $A = 3.485$ and $B = -3805$, determined from measurements for our atomic vapor cell, while the dashed line uses the parameters from ref. [5] ($A = 4.312$ and $B = -4040$) for the vapor pressure of liquid rubidium. In (b), the solid line shows the width computed from theory, with no adjustable parameters. The average error between the measurements and theory is 2.8%.

### B. Ring Cavity Scale Factor Enhancement

The tunable laser was used to scan over the modes of a rectangular ring cavity, of length $L = 42.64 \pm 0.01$ cm, derived from the measured free spectral range of the empty cavity, $703.0 \pm 0.1$ MHz. The temperature-stabilized Rb vapor cell, mounted within its oven, was placed within the optical path inside of the ring cavity. Figure 1 shows the optical layout for the unidirectional ring cavity measurements. The cavity consisted of three high reflectance mirrors and a 90:10 cube beamsplitter as the input coupler which also served as the output coupler in reflectance. Thus, for our cavity, $r_2 = 1$. The cavity modes were observed in reflectance. The combined cavity/vapor cell had a measured finesse of $7.6 \pm 1.3$, when detuned far from the absorption resonance. This value of finesse, and its uncertainty, are the mean and standard deviation of ten measured finesse values at the temperatures for which the scale factor enhancement was measured. The center frequency of the laser was adjusted to coincide with the peak of the composite $F = 2 \rightarrow F'$ resonance. The detuning between the cavity and atomic resonance was varied by an intracavity liquid-crystal variable retarder. The values of the two cavity parameters, $r_1$ and $a$, were found at each temperature

by a non-linear least squares fit of the theory to the reflection spectra for modes away from the resonance. The average values over all temperatures gave $r_1 = 0.946 \pm 0.006$ and $a = 0.674 \pm 0.044$, showing that these values were temperature-independent over the range of measured temperatures, 309–316 K.

For each temperature, spectra were recorded at a variety of detunings as a selected cavity mode was tuned across the atomic resonance via the liquid crystal. An automated peak finding program was used to obtain the frequencies of the mode peaks as well as their FWHM mode widths and modulation depths. For each temperature, the on-resonance scale factor enhancement, $S_0^{\Re}$, was determined by a model-independent fit of mode detunings vs. the empty-cavity mode detunings. Figure 4 (a) shows a typical fit of the $\triangle_p$ vs $\delta_p$ curve, for one temperature, using a linear fit to the central region near the resonance. We take the slope in this region to be the approximate value of $S_0^{\Re}$ for the given temperature, even though, strictly, $S_0^{\Re}$ is the slope exactly on resonance. Although the averaging involved in using a finite range of $\delta_p$ near zero for obtaining the slope will lower the value of $S_0^{\Re}$ slightly below what would be expected using an exact theoretical model of $\Delta_p$, the resulting error in $T_c$ is small compared to the expected temperature error. Figure 4(b) shows the measured dependence of $S_0^{\Re}$ on temperature, as well as the curve predicted from our theory, given by eq. 29. The scale factor pole from the measured $S_0^{\Re}$ data is obtained by fitting the data to a function which describes the behavior of $S_0(T)$ in a phenomenological manner,

$$S_0(T) = 1 - \frac{G}{(T - T_c)}, \tag{32}$$

where $G$ and $T_c$ are parameters to be determined from the fit. A fit to the $S_0^{\Re}(T)$ data shown in Fig. 4 yields $G = 6.93 \pm 0.67$ and $T_c = 315.23 \pm 0.18$ K. Our theoretical model for a Gaussian resonance, using the semi-empirical $\hat{\alpha}_0(T)$ and theoretical $\Gamma_\alpha^R(T)$ gives $T_c = 317.35$ K. The phenomenological expression in eq. 32 is also found to match very closely the theoretical expression from eq. 29 with proper selection of $G$, as shown in figure 4 (c).

## V. DISCUSSION OF RESULTS

Our semi-empirical model of the temperature-dependent absorption coefficient profile agrees with the data for the $^{87}$Rb $D_2$ $F = 2 \rightarrow F'$ resonance, within the experimental error. In particular, the peak absorption coefficient, $\alpha_0(T)$, from our model matches the

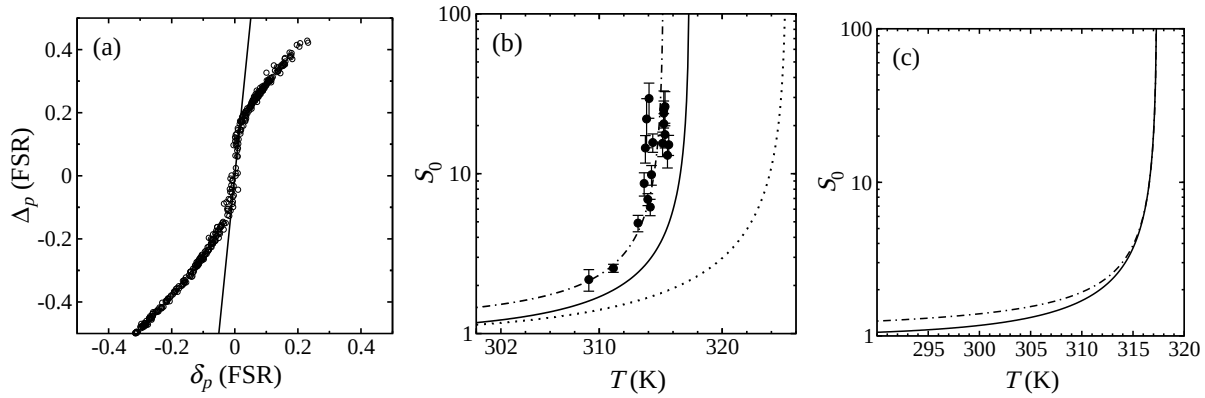


Figure 4. (a) Measurement of dispersive-cavity mode detuning ($\Delta_p$) vs empty cavity-mode detuning ($\delta_p$) from the $^{87}$Rb D$_2$ $F = 2 \rightarrow F'$ resonance at a vapor temperature of 314 K. The on-resonance scale factor enhancement, $S_0^{\Re}$, at this temperature is found by a linear fit to the data near resonance. (b) Comparison of the general analytical model prediction of $S_0^{\Re}$ vs $T$ for a Gaussian resonance (solid), computed using eq. 28 and eq. 15, with the measured values of $S_0^{\Re}$ (points), as in (a), at different temperatures. The dot-dash line is a fit to the data using the phenomenological expression, eq. 32, which gives the measured critcal temperature, $T_c = 315.23 \pm 0.18$K. Dotted line is the high-finesse model prediction of $S_0(T)$, from eq. 25. The general model predicts a critical temperature of $T_c = 317.35$K, and the high-finesse approximation predicts $T_c = 325.21$K. (c) Comparison of the phenomenological model of $S_0(T)$, (dot-dash line) eq. 32, with the exact theoretical expression, (solid line) eq. 29, using $G = 6.823$ and $T_c = 317.35$K.

experimental data over the entire temperature range of the measurement with an average error of less than 0.3%. The accuracy of the model indicates that the vapor pressure for an atomic vapor cell can be significantly different from the vapor pressure of liquid rubidium quoted in the literature[5, 6], but still follows the two-term equation 8. Thus, the $A$ and $B$ coefficients for the vapor pressure of the cell should be characterized in order to model the peak absorption coefficient accurately.

The measured resonance width versus temperature, $\Gamma_\alpha^R(T)$ is also in good agreement with the theory, with an average error across the measurement temperature range of 2.8%. We note that there are no adjustable parameters involved in the theory for $\Gamma_\alpha^R(T)$. Our theory neglected to include the natural linewidth contribution to the two-level transition width, although this contribution is built-in to our experimental determination of $\Gamma_\alpha(T)$. However, adding the natural linewidth contribution to the theory with an empirical relation

for the FWHM of a Voigt profile [12] only adds $2\pi(3.25\text{ MHz})$ to $\Gamma_\alpha(T)$, which reduces the discrepancy between the measurement and theory to 2.3% for $\Gamma^R_\alpha(T)$. At present, we do not believe our frequency scale for the measurements has such a large error. A rather large error in the measured temperature of the vapor, $\approx 20$ K, would be required to explain the discrepancy in $\Gamma^R_\alpha(T)$. Although our measurement of the oven temperature may differ from the vapor temperature, for example, near the end caps of the oven, such a large systematic error in the vapor temperature is not expected, and, in any case, would not be consistent with our results for $\alpha_0(T)$.

Additional checks were made to determine the source of the broadening of the experimental values of $\Gamma^R_\alpha(T)$. We considered Zeeman effects from the oven heater current and artificial broadening of the transmittance profile from the detection bandwidth of the measurement system. Both of these potential sources have been ruled out. A possible explanation for the extra broadening of the resonance observed in the experiment is that the ground state sublevel thermalization time in the vapor cell is longer than the mean time between wall collisions. As a result, the individual contributions of the $2 \rightarrow F'$ transitions to the resonance profile would not be exactly in the ratios given by $s(2, F')$, leading to a composite resonance which could be slightly broader than that of the theory for $\alpha_F(\Delta, T)$ in eq. 15. We note, however, that the additional resonance broadening of 2.3% in the measurements has a small effect on the comparison between the predicted and observed scale factor enhancement, increasing the predicted critical temperature by only 0.21 K, well within the vapor temperature uncertainty.

The uni-directional ring cavity experiment demonstrates that $S_0$ can be tuned with temperature, from nearly unity to past the pole in $S_0$. For the low finesse cavity used in our experiment, it is clear from Fig. 4 that the high finesse approximation result for $S_0(T)$, given by eq. 25, gives a large error of about 10 K in the critical temperature for $S_0$. Using our measured cavity parameters, $L$, $r_1$, and $a$, within the general expression of eq. 29 gives a critical temperature which is different from that estimated from the cavity measurements by about 2 K. Although the atomic resonance used for this experiment is not a symmetric Gaussian resonance, due to its composite nature, eq. 29 nevertheless provides an estimate of the critical temperature which is approximately within the systematic uncertainity in our atomic vapor temperature, indicating that the asymmetric resonance shape contributes only a small correction to $T_c$.

For atomic vapor cells as the intracavity dispersive media, the rapid change of $S_0(T)$ with temperature near the scale factor pole limits the useful scale factor enhancement, given the practical limitations of stabilizing the atomic vapor temperature. The relevant figure of merit is the variation in $S_0(T)$ for a given variation of temperature, $\delta T$. We compute

$$\frac{\delta S_0}{S_0}(T) \;=\; \frac{\delta T}{S_0}\left(\frac{dS_0}{dT}\right). \tag{33}$$

Calculation of this quantity may be done directly by computing eq. 28 or eq. 29, and obtaining its numerical derivative. However, it is easier to use the phenomenological expression for $S_0(T)$ from eq. 32. Then, for $S_0 \gg 1$, we find,

$$\left|\frac{\delta S_0}{S_0}\right|(T) \;=\; \left|\frac{\delta T}{T - T_c}\right|. \tag{34}$$

Using the predicted value of $T_c = 317.35$ K for our experimental parameters, and an estimated temperature stability value of $\delta T \approx 10$ mK, we obtain for the specific cavity/vapor-cell system used in our work,

$$\left|\frac{\delta S_0}{S_0}\right|(T) \;=\; \left|\frac{0.01}{T - 317.35}\right|, \tag{35}$$

showing the expected result that the fractional stability of $S_0$ decreases rapidly as we approach the scale factor pole. For temperature tuning of the scale factor enhancement alone, the above expression provides the operating temperature of the vapor cell for the desired fractional scale factor stability. For example, to obtain a scale factor stability of $10^{-4}$, the operating temperature for our system is computed to be 217.35 K, which limits $S_0$ to unity, even if such an operating temperature was practically realizable. Relaxing the scale factor stability by two orders of magnitude gives a more realistic operating temperature of 316.35 K, for which the theory predicts $S_0 = 7.76$.

The primary limitation for operating simultaneously at high scale factor enhancement and with high scale factor stability for our dispersive medium is the achievable temperature stability of the vapor, owing mainly to the strong dependence of the peak absorption coefficient on temperature in typical atomic vapor cells. Indeed, whenever the anomalous dispersion depends on the atom density[2, 13], the scale factor stability is likely to be limited by the temperature stability of the vapor. However, the temperature-stability limitation will be less severe with respect to achieving large $S_0$ when another scale factor tuning parameter, $p$, is accessible. For example, with the use of side optical pumping to increase $\alpha_0$, as in [1],

$p$ can represent the intensity of the optical pumping beam, so that $S_0$ is now a function of both $p$ and $T$. Then,

$$\delta S_0(p,T) \;=\; \left(\frac{\partial S_0}{\partial p}\right)\delta p \;+\; \left(\frac{\partial S_0}{\partial T}\right)\delta T \tag{36}$$

and the operating temperature can now be chosen at a much lower temperature where $\partial S_0/\partial T$ is considerably smaller, and the contribution to $\delta S_0$ from the $(\partial S_0/\partial p)\delta p$ term can be made much smaller due to stabilization of $p$. As an example, in our earlier work [1], we demonstrated using optical pumping to tune $S_0$ from unity through the pole at room temperature, $\approx$ 300 K. Thus, with perfect stabilization of the pump beam intensity, $\delta p = 0$, and $\delta T = 10$ mK, the fractional scale factor stability, $\delta S_0/S_0$, can reach $6 \times 10^{-4}$ at room temperature, for any value of $S_0$, according to eq. 35.

## VI. SUMMARY

We obtained a theoretical expression for the on-resonance cavity scale factor enhancement, $S_0(T)$, for an ideal Gaussian absorption resonance. In order to quantify the correspondence of the theory with the dispersion enhancement provided by an intracavity atomic vapor cell, we measured the absorption coefficient profile versus temperature for the $^{87}$Rb $D_2$ $F = 2 \rightarrow F'$ resonance and obtained the Gaussian resonance parameters as a function of temperature. A semi-theoretical model of the absorption coefficient profile for a composite set of Doppler-broadened hyperfine transitions, applicable to alkali atom vapor cells, was demonstrated to give good agreement with our experimental results for $\alpha_0(T)$ and $\Gamma_\alpha^R(T)$. Although measurements of these resonance parameters alone would have sufficed to test our model of $S_0(T)$, establishing a detailed and careful connection to the theory of optical transitions in thermal atomic vapors is useful generally, for cases where vapor cells of other atomic species, e.g. cesium, are used as intracavity dispersive media. Our results indicate that atom density as a function of temperature inside of an atomic vapor cell deviates from ideal conditions of vapor pressure from a liquid reservoir at a given temperature. We find that determination of the $A$ and $B$ parameters in the vapor pressure model for the atomic vapor cell is necessary to match the experimental absorption coefficient profiles with the theory. A direct comparison of measurements of $S_0(T)$ with those computed by our theoretical expression for a ring optical cavity with arbitrary finesse showed close correspondence with the predicted critical temperature, within 2 K of that indicated by the measurements.

In gyro applications for navigation, scale factor stabilities of better than $10^{-5}$ are required to be competitive with currently available systems. Our experimental and theoretical results show that the Doppler-broadened resonance used in our $^{87}$Rb atomic vapor cell is severely limited in its usefulness for dispersion-enhanced optical cavity-based sensors when temperature tuning is used to achieve high scale factor enhancement values. We find, for the cavity/vapor cell system used here, that a scale factor stability of $10^{-4}$ is not achievable, while a scale factor stability of $10^{-2}$ can only be achieved for $S_0 < 8$. However, our results do not rule out the possibility of simultaneously achieving both high scale factor stability and high values of $S_0$ for other tuning methods, e.g. optical pumping tuning of $S_0$. For operation at room temperature and vapor temperature stability of 10 mK, the temperature-dependence of our vapor cell resonance parameters imposes a limit on the scale factor stability of about $6 \times 10^{-4}$ for any tuning method and value of $S_0$.

The atomic vapor cell was selected as the dispersive medium for our initial experiments on scale factor enhancement in an optical cavity [1, 9] due to the exceptional frequency stability of its resonances. Our present work indicates the need to explore other resonant systems with narrow, frequency-stable resonances, but with better dispersion stability than the type of atomic vapor cell used here. Alternatively, a feedback control method for stabilizing the resonant atom density in a vapor cell may provide higher stability than that achievable with temperature stabilization alone[14]. Another interesting possibility is the use of laser cooled and trapped atoms as the intracavity dispersion medium, for which the temperature stability issue disappears. Such a system allows tuning of the atom density by non-thermal control and provides absorption resonances at the natural linewidth, suitable for cavities with a finesse greater by a factor of 100. We plan to explore this idea in a future paper on the fundamental quantum sensitivity limit of the dispersion-enhanced passive ring cavity.

## ACKNOWLEDGMENTS

K.M. and D.D.S were supported by the U.S. Army AMRDEC Navigation Technologies Group. D.D.S., H.C., and H.A.L. were supported by the NASA Game Changing Technologies (GCT) Office, Fast-Light Optical Gyroscopes program. We wish to thank Mr. Brian Grantham for a useful discussion on present-day gyroscope technology, and Dr. Shawn

Pethel for a careful reading of the manuscript.

---

[1] Myneni, K., Smith, D.D., Odutola, J.A., Schambeau, C.A., Phys. Rev. A **85**. 063813 (2012).

[2] Yum, H.N., Salit M., Yablon, J., Salit, K., Wang Y., Shahriar, M.S., Opt. Express **18**, 17658 (2010).

[3] M. Salit and M.S. Shahriar, J. Opt. **12**, 104014 (2010).

[4] J. Scheuer and M.S. Shahriar, Opt. Lett. **38**, 3534 (2013).

[5] Alcock, C.B., Itkin, V.P., and Horrigan, M.K., Candian Metallurgical Quarterly **23**, 309 (1984).

[6] Daniel A. Steck, "Rubidium 87 D Line Data," available online at `http://steck.us/alkalidata` (revision 2.1.2, 12 August 2009).

[7] M. Rozwadowski and E. Lipworth, J. Chem. Phys. **43**, 2347 (1965).

[8] B. Gao, Phys. Rev. A **48**, 2443 (1993).

[9] Smith, D.D., Myneni, K., Odutola, J.A., Diels, J.C., Phys. Rev. A **80**, 011809(R) (2009).

[10] Smith, D.D., Myneni, K., Chang, H., Proc. SPIE **8636**, 86360F (2013).

[11] Davis, S.J., Rawlins, W.T., Galbally-Kinney, K.L., and Kessler, W.J., Proc. SPIE **7196**, 71960G (2009).

[12] J. J. Olivero and R. L. Longbothum, J. Quant. Spectrosc. Radiat. Transfer **17**, 233–236 (1977).

[13] Phillips, N.B., Novikova, I., Mikhailov, E.E., Budker, D., Rochester, S., J. Mod. Opt. **60**, 64 (2013).

[14] Bogi, A., Marinelli, C., Burchianti, A., Mariotti, E., Moi, L., Gozzini, S., Marmugi, L., Lucchesini, A., Opt. Lett. **34**, 2643 (2009).